Counterdiabatic mode-evolution based coupled-waveguide devices

Shuo-Yen Tseng

[1]*Department of Photonics, National Cheng Kung University, Tainan, Taiwan*
[2]*Advanced Optoelectronic Technology Center, National Cheng Kung University, Tainan, Taiwan*
[*]*tsengsy@mail.ncku.edu.tw*

Abstract: The goal in designing mode-evolution based devices is to realise short and high-fidelity components. The counterdiabatic protocol in coherent quantum state control can be used to cancel unwanted coupling between adiabatic modes in mode evolution but is not directly realisable in the coupled-waveguide system. By finding alternative coupled-mode equations that links to the same interaction picture dynamical equation as the counterdiabatic protocol via unitary transformations, we have derived a universal formalism for the design of short and high-fidelity mode-evolution based coupled-waveguide devices. Starting from a traditional adiabatic device design, the counterdiabatic protocol leads to a high-fidelity device, with its evolution following the adiabatic modes exactly even when the adiabatic condition is violated. Tolerance analysis shows that the counteradiabatic devices combine the advantages of adiabatic and resonant devices. The formalism is used to design asymmetric waveguide couplers.

OCIS codes: (130.3120) Integrated optics devices; (130.2790) Guided waves; (060.1810) Buffers, couplers, routers, switches, and multiplexers; (000.1600) Classical and quantum physics.

References and links

1. R. R. A. Syms, "The digital directional coupler: improved design," IEEE Photon. Technol. Lett. **4,** 1135-1138 (1992).
2. X. Sun, H.-C. Liu, and A. Yariv, "Adiabaticity criterion and the shortest adiabatic mode transformer in a coupled-waveguide system," Opt. Lett. **34,** 280-282 (2009).
3. M. R. Watts, H. A. Haus, and E. P. Ippen, "Integrated mode-evolution-based polarization splitter," Opt. Lett. **30,** 967-969 (2005).
4. M. V. Berry, "Histories of adiabatic quantum transitions," Proc. R. Soc. Lond. A **429**, 61-72 (1990).
5. S. Guérin, S. Thomas, and H. R. Jauslin, "Optimization of population transfer by adiabatic passage," Phys. Rev. A **65,** 023409 (2002).
6. M. G. Bason, M. Viteau, N. Malossi, P. Huillery, E. Arimondo, D. Ciampini, R. Fazio, V. Giovannetti, R. Mannella, and O. Morsch, "High-fidelity quantum driving," Nature Phys. **8,** 147-152 (2012).
7. B. T. Torosov, S. Guérin, and N. V. Vitanov, "High-fidelity adiabatic passage by composite sequence of chirped pulses," Phys. Rev. Lett. **106,** 233001 (2011).
8. R. G. Unanyan, L. P. Yatsenko, K. Bergmann, and B. W. Shore, "Laser-induced adiabatic atomic reorientation with control of diabatic losses," Opt. Commun. **139,** 48-54 (1997).
9. M. Demirplak and S. A. Rice, "Adiabatic population transfer with control fields," J. Phys. Chem. A **107,** 9937-9945 (2003).
10. M. Demirplak and S. A. Rice, "Assisted adiabatic passage revisited," J. Phys. Chem. B **109,** 6838-6844 (2005).
11. M. V. Berry, "Transitionless quantum driving," J. Phys. A: Math. Theor. **42,** 365303 (2009).
12. X. Chen, I. Lizuain, A. Ruschhaupt, D. Guéry-Odelin, and J. G. Muga, "Shortcut to adiabatic passage in two- and three-level atoms," Phys. Rev. Lett. **105,** 123003 (2010).

#195633 - $15.00 USD Received 12 Aug 2013; accepted 19 Aug 2013; published 3 Sep 2013

13. T.-Y. Lin, F.-C. Hsiao, Y.-W. Jhang, C. Hu, and S.-Y. Tseng, "Mode conversion using optical analogy of shortcut to adiabatic passage in engineered multimode waveguides," Opt. Express **20,** 24085-24092 (2012).
14. S. Longhi, "Quantum-optical analogies using photonic structures," Laser and Photon. Rev. **3,** 243-261 (2009).
15. S. K. Korotky, "Three-space representation of phase-mismatch switching in coupled two-state optical systems," IEEE J. Quantum Electron. **22,** 952-958 (1986).
16. S. Ibáñez, X. Chen, E. Torrontegui, J. G. Muga, and A. Ruschhaupt, "Multiple Schrödinger pictures and dynamics in shortcuts to adiabaticity," Phys. Rev. Lett. **109,** 100403 (2012).
17. A. Yariv, "Coupled-mode theory for guided-wave optics," IEEE J. Quantum Electron. **9,** 919-933 (1973).
18. K. Okamoto, *Fundamentals of Optical Waveguides* (Academic, 2006).
19. K. Kawano and T. Kitoh, *Introduction to Optical Waveguide Analysis: Solving Maxwell's Equations* (Wiley, 2001).
20. Y. Bai, Q. Liu, K. P. Lor, and K. S. Chiang, "Widely tunable long-period waveguide grating couplers," Opt. Express **14,** 12644-12654 (2006).
21. A. Syahriar, V. M. Schneider, and S. Al-Bader, "The design of mode evolution couplers," J. Lightwave Technol. **16,** 1907-1914 (1998).
22. S.-Y. Tseng and M.-C. Wu, "Mode conversion/splitting by optical analogy of multistate stimulated Raman adiabatic passage in multimode waveguides," J. Lightwave Technol. **28,** 3529-3534 (2010).

1. Introduction

Mode-evolution based coupled-waveguide devices have been widely used in optical communications to transfer light between different components. For example, two-by-two couplers [1], mode transformers [2], and polarisation splitters [3] have been proposed or demonstrated in integrated optics. The idea behind mode-evolution based devices is to have the system following adiabatically the local eigenmodes of the device while minimising coupling of the eigenmodes, and the devices generally have more relaxed fabrication tolerances and larger bandwidth. However, these devices have to be sufficiently long to satisfy the adiabatic condition [4]. Otherwise, unwanted coupling among the adiabatic modes would deteriorate the device performance. Long device length also reduces device density and induces more transmission losses.

A universal adiabaticity criterion for designing mode-evolution based coupled-waveguide device has recently been derived by analysing the power coupling between the adiabatic modes [2]. The criterion also gives the shortest length of a mode-evolution based coupled-waveguide device for a given maximal tolerance. In addition to length reduction, the other requirement in the design of mode-evolution based coupled-waveguide devices is to obtain the desired output mode with the highest fidelity, that is, to obtain the highest coupling/transformation/conversion efficiency. In nearly all adiabatic mode-evolution devices, the efficiency is close to, but less than 1. The ultimate goal in component design is thus to realise short and high-fidelity mode-evolution based devices. The problem at hand is analogous to the problem of coherent quantum system state control, with the goal of performing fast state control with high-fidelity. Several methods have been proposed for high-fidelity quantum system driving [5–12]. The counterdiabatic [8–12] protocol ensures a perfect and fast following of the adiabatic states, and its optical realisation has been proposed in multimode waveguide mode converters using long-period gratings [13]. The approach of this paper is based on the similarity between the scalar and paraxial wave equation describing spatial light propagation in weakly-coupled waveguide structures and the Schrödinger equation describing temporal quantum states evolution in a system driven by external electromagnetic fields, with the Hamiltonian $\mathbf{H}_0$ related to waveguide geometries [14]. The above Schrödinger picture representation can be linked to the interaction picture by a unitary transformation $\mathbf{U}$, and the interaction picture Hamiltonian is $\mathbf{H}_I = \mathbf{U}^\dagger(\mathbf{H}_0 - \mathbf{K})\mathbf{U}$, with $\mathbf{K} = i\hbar\dot{\mathbf{U}}\mathbf{U}^\dagger$. When $\mathbf{K}$ is negligible, the adiabatic approximation is valid, and the system follows the eigenstates of $\mathbf{H}_0$ closely. The counterdiabatic protocol adds the counterdiabatic term $\mathbf{H}_{cd} = \mathbf{K}$ to $\mathbf{H_0}$ to cancel any coupling between the adiabatic states such that the system follows the eigenstates of $\mathbf{H}_0$ perfectly even for short process times [8, 9].

There exists, however, a problem in realising the counterdiabatic protocol in coupled-

#195633 - $15.00 USD Received 12 Aug 2013; accepted 19 Aug 2013; published 3 Sep 2013

waveguide devices. The straightforward application of the protocol results in coupling terms that require non-zero imaginary part in the coupling coefficient, which is not realisable in a linear coupled-waveguide system [15]. It is recently suggested that a common interaction picture dynamical equation can correspond to multiple Schrödinger equations that represents different physical processes [16]. In this paper, we show that, by proper unitary transformations, the counterdiabatic protocol can be transformed into a Schrödinger picture Hamiltonian that is physically realisable in coupled-waveguide systems. The formalism is applicable to the design of short and high-fidelity mode-evolution based coupled-waveguide devices.

2. Theoretical analysis

2.1. Coupled-mode equations

The theory described in this paper can be applied in general to weakly-coupled waveguide structures described by the coupled-mode theory [17]. For the convenience of theoretical derivation, we consider the coupled-waveguide system shown schematically in Fig. 1. It consists of two waveguides, waveguide 1 and waveguide 2, placed in proximity with propagation constants β_1 and β_2. The refractive index or geometry of the two waveguides are allowed to vary along the propagation direction z. Light is coupled into the device at $z = 0$ and out at $z = L$. Under the scalar and paraxial approximation and assuming weak coupling [18], the changes in the guided-mode amplitudes in the individual waveguides $[A_1, A_2]^T$ with propagation distance is described by coupled-mode equations as

$$\frac{d}{dz}\begin{bmatrix} A_1 \\ A_2 \end{bmatrix} = -i\begin{bmatrix} \Delta & \kappa \\ \kappa & -\Delta \end{bmatrix}\begin{bmatrix} A_1 \\ A_2 \end{bmatrix} = -i\mathbf{H_0}\begin{bmatrix} A_1 \\ A_2 \end{bmatrix}, \tag{1}$$

where κ (real) is the coupling coefficient, and $\Delta = (\beta_1 - \beta_2)/2$ describes the degree of mismatch between the waveguides. Replacing the spatial variation z with the temporal variation t, (1) is equivalent to the time-dependent Schrödinger equation ($\hbar = 1$) describing the interaction dynamics of a two-state system driven by a coherent laser excitation, and $\mathbf{H}_0$ is the Hamiltonian. $\mathbf{H}_0$ can be written in terms of Pauli spin matrices as $\mathbf{H}_0 = \kappa\sigma_x + 0\sigma_y + \Delta\sigma_z$ and mapped to a real three dimensional space as a rotation vector $\mathbf{\Omega}_0 = [\kappa, 0, \Delta]^T$. When the input state coincides with $\mathbf{\Omega}_0$, adiabatic evolution is achieved with $\mathbf{H}_0$ by slowly varying κ and Δ so that the system state follows $\mathbf{\Omega}_0$ collinearly to a final state with motion on the $x-z$ plane. If the adiabatic condition is not satisfied, the system state cannot follow $\mathbf{\Omega}_0$, resulting in low conversion efficiency. Also, we note that the adiabatic following is an approximation. Even if the adiabaticity criterion is satisfied, efficiency is generally close to, but less than 1.

2.2. Counterdiabatic term

A counterdiabatic term can be constructed to undo the effects of nonadiabaticity on the state evolution and obtain short and high-fidelity conversion [9]. We consider the interaction picture constructed using the adiabatic basis $|a_n\rangle$ that diagonalises $\mathbf{H}_0$ so that $\mathbf{U} = \sum |a_n\rangle\langle a_n|$. The counterdiabatic term thus obtained is

$$\mathbf{H}_{cd} = i\hbar\dot{\mathbf{U}}\mathbf{U}^\dagger = \frac{1}{2}\begin{bmatrix} 0 & i\kappa_a(z) \\ -i\kappa_a(z) & 0 \end{bmatrix} = \frac{1}{2}\kappa_a\sigma_y, \tag{2}$$

with $\kappa_a(z) = (\dot{\kappa}\Delta - \dot{\Delta}\kappa)/(\kappa^2 + \Delta^2)$. The counterdiabatic protocol Hamiltonian is thus $\mathbf{H}_0 + \mathbf{H}_{cd} = \kappa\sigma_x + (1/2)\kappa_a\sigma_y + \Delta\sigma_z$, corresponding to a rotation vector $\mathbf{\Omega}_{cd} = [\kappa, \frac{1}{2}\kappa_a, \Delta]^T$. However, for linear coupled-waveguide system, the rotation vector is confined to the $x-z$ plane [15], rendering the counterdiabatic protocol not physically realisable.

#195633 - $15.00 USD Received 12 Aug 2013; accepted 19 Aug 2013; published 3 Sep 2013

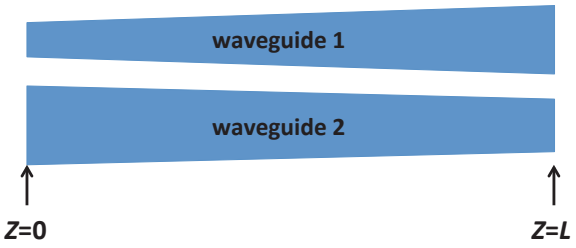

Fig. 1. Schematic of the mode-evolution coupled-waveguide system.

2.3. *Unitary transformation*

We can construct the physically realisable counteradiabatic protocol by recasting $\mathbf{H}_0+\mathbf{H}_{cd}=\kappa\sigma_x+\frac{1}{2}\kappa_a\sigma_y+\Delta\sigma_z$ in the form $\kappa_s\sigma_x+\Delta_s\sigma_z$, eliminating the need for non-zero imaginary part in the coupling coefficient. For the coupled-waveguide system, the required transformation can be obtained by observing that a rotation around the z-axis will bring Ω_{cd} back to the $x-z$ plane. Write

$$\mathbf{H}_0+\mathbf{H}_{cd}=\begin{bmatrix}\Delta & ke^{-i\phi}\\ ke^{i\phi} & -\Delta\end{bmatrix}, \tag{3}$$

where $\phi=tan^{-1}(\kappa_a/2\kappa)$ and $k=\sqrt{\kappa^2+(\kappa_a/2)^2}$, we can apply the z-axis rotation [6]

$$\mathbf{U}_z=\begin{bmatrix}e^{-i\phi/2} & 0\\ 0 & e^{i\phi/2}\end{bmatrix}, \tag{4}$$

hence the interaction picture Hamiltonian becomes

$$\mathbf{U}_z^{\dagger}(\mathbf{H}_0+\mathbf{H}_{cd}-i\hbar\dot{\mathbf{U}}_z\mathbf{U}_z^{\dagger})\mathbf{U}_z=\kappa_s\sigma_x+\Delta_s\sigma_z, \tag{5}$$

with $\kappa_s=k=\sqrt{\kappa^2+(\kappa_a/2)^2}$ and $\Delta_s=\Delta-(1/2)\dot{\phi}$. It can be regarded as a Schrödinger picture Hamiltonian, and together with (3), link to the same interaction picture Hamiltonian. Casted in the new basis, it can now be realised using the coupled-waveguide system and guarantees the same fast and high-fidelity mode evolution described by $\mathbf{H}_0+\mathbf{H}_{cd}$.

2.4. *The counterdiabatic coupler*

For an adiabatic coupler originally designed with coupling coefficient κ and mismatch Δ, the mode evolution cannot follow the adiabatic modes when the adiabatic condition is not satisfied, and the fidelity is close to, but less then 1. From the above analysis, the corresponding counterdiabatic coupler designed using the counterdiabatic formalism with coupling coefficient κ_s and mismatch Δ_s would follow the adiabatic eigenmodes of $\mathbf{H}_0$ perfectly to ensure fast and high-fidelity coupling. In the following numerical analysis, we use examples to show how these formulas can be used to obtain parameters directly related to waveguide structures for device design.

3. Numerical analysis

3.1. *Adiabatic following*

We numerically solve (1) using the common adiabatic formalism and the corresponding counterdiabatic formalism at different device lengths. For the common adiabatic devices, the

#195633 - $15.00 USD Received 12 Aug 2013; accepted 19 Aug 2013; published 3 Sep 2013

mode evolution follows one of the eigenmodes of the device to transfer power from one waveguide to the other. One strategy to minimise the coupling between the eigenmodes is to design the taper functions such that the separation of the eigenvalues is the maximum value allowed by the system throughout the evolution. Since the local eigenvalues of $\mathbf{H}_0$ are $\pm\sqrt{\Delta^2+\kappa^2}$, we can then put $\kappa=\kappa_0\sin\theta$ and $\Delta=\kappa_0\cos\theta$ [1]. When the adiabatic condition $\frac{1}{2}|(\kappa\dot{\Delta}-\dot{\kappa}\Delta)/(\kappa^2+\Delta^2)|\ll|\sqrt{\kappa^2+\Delta^2}|$ [12], is satisfied, the corresponding solution for the powers in the individual waveguides $[|A_1(z)|^2,|A_2(z)|^2]$ follows approximately the eigenmode power evolution given by $[\cos^2(\theta/2),\sin^2(\theta/2)]$ in the limit $\kappa_0 L\to\infty$.

Many different taper functions have been proposed for the design of θ, for illustrative purposes, we choose a linear function $\theta=\pi z/L$, where L is the device length. With this choice of taper function, we obtain the adiabatic condition as $L\gg\frac{\pi}{2\kappa_0}$. Assuming $\kappa_0=1$ mm^{-1}, corresponding to the adiabatic condition of $L\gg\frac{\pi}{2}$ mm, we calculate the fraction of power in the waveguides by solving (1) with the Hamiltonian $\mathbf{H}_0$ and using $[A_1(0),A_2(0)]^T=[1,0]^T$ as the input. The results of fractional power evolution for different device lengths are shown in Fig. 2 (dash-dotted lines). The solid lines are the theoretical eigenmode power evolution given by $[\cos^2(\theta/2),\sin^2(\theta/2)]$. It is clear that as the device length increases, the power evolution follows the eigenmode more closely, and the coupling efficiency at the output is closer to 1. At shorter lengths, some large ripples can be seen, indicating scattering of power from one eigenmode into the other. Small ripples can still be seen even for the 50 mm device.

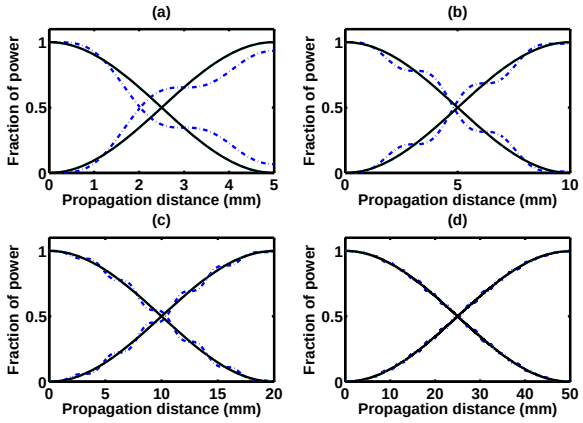

Fig. 2. Fractional power evolution in the two waveguides for different device lengths. (a) 5 mm, (b) 10 mm, (c) 20 mm, and (d) 50 mm. Dash-dotted lines show the adiabatic coupler corresponding to $\mathbf{H}_0$. Solid lines show the counterdiabatic coupler corresponding to $\kappa_s\sigma_x+\Delta_s\sigma_z$. The solid lines also overlay the theoretical eigenmode power evolution curves given by $[\cos^2(\theta/2),\sin^2(\theta/2)]$.

3.2. Counterdiabatic following

Then, we implement the counteradiabatic formalism given in (5) by replacing the Hamiltonian in (1) with $\kappa_s\sigma_x+\Delta_s\sigma_z$. Solving (1) using $[A_1(0),A_2(0)]^T=[1,0]^T$ as the input, the results are also shown in Fig. 2 (solid lines). The fractional power evolution coincides with the eigenmode completely for every device length, demonstrating high-fidelity power coupling predicted by the theory. To illustrate the magnitude of coupling and waveguide mismatch required to implement the counterdiabatic formalism, we show the required κ_s and Δ_s for the four device lengths considered in Fig. 3 (solid lines). Also shown in the figure are the associated $\kappa=\kappa_0\sin\theta$ and

#195633 - $15.00 USD Received 12 Aug 2013; accepted 19 Aug 2013; published 3 Sep 2013

$\Delta = \kappa_0 \cos\theta$ of the original adiabatic devices (dashed lines). To implement the counterdiabatic formalism in a coupled waveguide system shown in Fig. 1, one designs the waveguide separation as a function of z to realise the coupling coefficient κ_s, and the waveguide widths are adjusted as a function of z to achieve the required mismatch Δ_s. From Fig. 3(a), we can see that when the device length is short, the required additional coupling and mismatch are also increased throughout the device; thus putting a limit on the physically realisable shortest length of the counterdiabatic coupler depending on the chosen waveguide platform. For longer device lengths in Figs. 3(b)–3(d), additional coupling and mismatch at the beginning and the end of the device are sufficient to cancel the ripples seen in Figs. 2(b)–2(d).

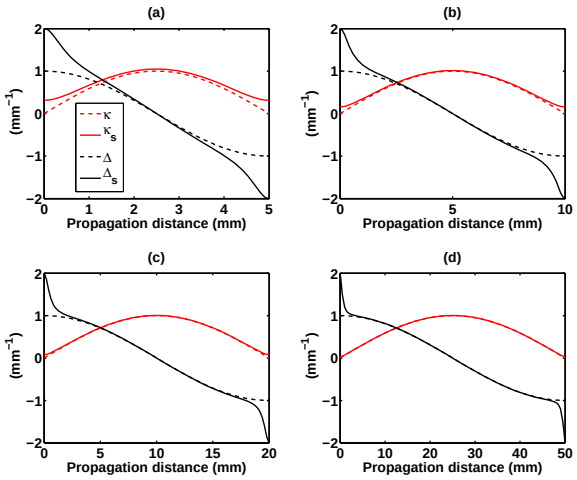

Fig. 3. κ_s and Δ_s for the four device lengths considered in Fig. 2. (a) 5 mm, (b) 10 mm, (c) 20 mm, and (d) 50 mm. Red solid lines indicate the coupling coefficients for the counterdiabatic couplers. Black solid lines indicate the waveguide mismatch for the counterdiabatic couplers. Red dashed lines are the coupling coefficients for the adiabatic couplers. Black dashed lines are the waveguide mismatch for the adiabatic couplers.

Next, we calculate the coupling efficiency variation with device length. The coupling efficiency from waveguide 1 to waveguide 2 for the adiabatic coupler (dash-dotted) and the counterdiabatic coupler (solid) are shown in Fig. 4. It is clear that the curve for the adiabatic coupler have sidelobes, indicating the possibility of obtaining less than perfect fidelity even for long device lengths. On the other hand, the counterdiabatic coupler achieves complete coupling for any device length, showing the desired properties of short and high-fidelity mode-evolution based coupled-waveguide devices. In this analysis, no limits are put on the coupling coefficient and mismatch of the coupler to account for physical realisability of the devices. Once a particular waveguide system is chosen, practical considerations such as the achievable coupling gap would limit the coupling coefficient and mismatch of the practical design. The device length cannot be reduced indefinitely. As long as the required coupling and mismatch can be realised with the chosen waveguide system at a particular length, the counterdiabatic formalism always ensures perfect fidelity.

From the above analysis, we can see that the counterdiabatic formalism works to ensure perfect fidelity and exact following of the original adiabatic eigenmodes when the adiabatic condition is satisfied; and when the adiabatic condition is not satisfied, its additional coupling also works to ensure complete power transfer. For the traditional adiabatic couplers, the adia-

#195633 - $15.00 USD Received 12 Aug 2013; accepted 19 Aug 2013; published 3 Sep 2013

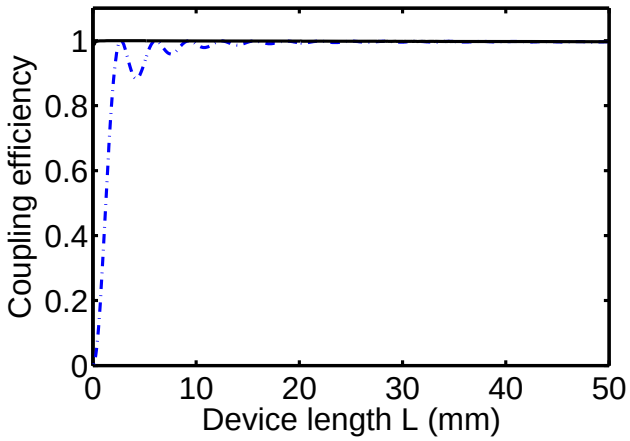

Fig. 4. Coupling efficiency as a function of the device length L. (Dash-dotted line) adiabatic coupler. (Solid line) counterdiabatic coupler.

baticity of the device can be improved by increasing its coupling strength as well. For example, the adiabatic condition for the devices discussed above reads $L \gg \frac{\pi}{2\kappa_0}$. By increasing the coupling strength κ_0, the adiabatic condition can be satisfied at shorter device lengths. However, even with the increased coupling, the device still works under the adiabatic approximation. That is, the fidelity will be close to but not equal to 1, and the ripples seen in the dash-dotted lines in Fig. 2 will remain. On the other hand, the counterdiabatic formalism works to cancel all unwanted coupling between adiabatic modes in mode evolution so that the fidelity is always perfect.

3.3. Comparison with adiabatic and resonant design schemes

While the addition of $\mathbf{H}_{cd}$ might seem a daunting task in quantum system state control because the level of control needed over laser pulse parameters in order to implement the time-dependent κ_a, the implementation of the counterdiabatic formalism in coupled-waveguide system is straightforward with modern fabrication technologies. Apparently, κ_s and Δ_s depend on $\mathbf{H}_0$, and some control of the waveguide parameters over the propagation distance is required to implement the counterdiabatic design. We know that adiabatic designs requires less precise control over waveguide parameters, while on the opposite end, resonant coupling techniques require very precise definition of the coupling length and coupling coefficient [18]. So the question that naturally arises is: how does the counteradiabatic coupler compare with the adiabatic coupler and the resonant coupler in terms of robustness to waveguide parameter variations?

Before answering this question, we first note that the counterdiabatic term $\mathbf{H}_{cd}$ in (2) itself drives the system along the eigenstates of $\mathbf{H}_0$ exactly [12], and the system characteristics of a system driven by $\mathbf{H}_{cd}$ are the same as a resonantly coupled device [8]. So, we consider the system tolerance to coupling coefficient variations for different device lengths by numerically solving (1) for three cases: (a) the adiabatic coupler described by $\mathbf{H}_0$, (b) the counterdiabatic coupler described by $\mathbf{H}_0 + \mathbf{H}_{cd}$, and (c) the resonant coupler described by $\mathbf{H}_{cd}$. The design parameters are fixed for all three cases at every device length. The coupling efficiencies from waveguide 1 to waveguide 2 subject to $\pm 50\%$ variations in coupling coefficients uniformly along the couplers for all three cases are shown in Fig. 5. The adiabatic coupler in Fig. 5(a) shows good tolerance to coupling coefficient variations when the device length is long enough.

#195633 - $15.00 USD Received 12 Aug 2013; accepted 19 Aug 2013; published 3 Sep 2013

And the ripples seen in the figure indicates less than 1 fidelity due to coupling between the adiabatic modes. As expected, the tolerance of the resonant coupler in Fig. 5(c) is inferior to the other two couplers, and its characteristics can be described by the square of a sinusoidal function [18]. The results for the counterdiabatic coupler are shown in Fig. 5(b). At the short length extreme, its tolerance is the same as the resonant coupler. This is expected because $\mathbf{H}_{cd}$ is dominant. As the device length increases, the tolerance of counterdiabatic couplers exceeds that of resonant couplers and is comparable to the adiabatic couplers; at the same time, the ripples seen in adiabatic couplers are reduced, indicating higher fidelity than adiabatic couplers. For even longer device lengths, the tolerance of counterdiabatic couplers becomes the same as adiabatic couplers because $\mathbf{H}_0$ is dominant now. The level of waveguide parameter engineering required to implement the counterdiabatic scheme is on the same level of resonant designs in the short device length limit. For the intermediate length, the engineering requirement is relaxed to the level of adiabatic designs, and the fidelity is improved. For the longer device length, the engineering requirement is the same as adiabatic devices. So, the counterdiabatic coupler provides a high-fidelity and robust transition from the short but not robust resonant coupler to the long but robust adiabatic coupler. Of course, the price to pay is the extra coupling strength and mismatch needed to implement the counterdiabatic term $\mathbf{H}_{cd}$.

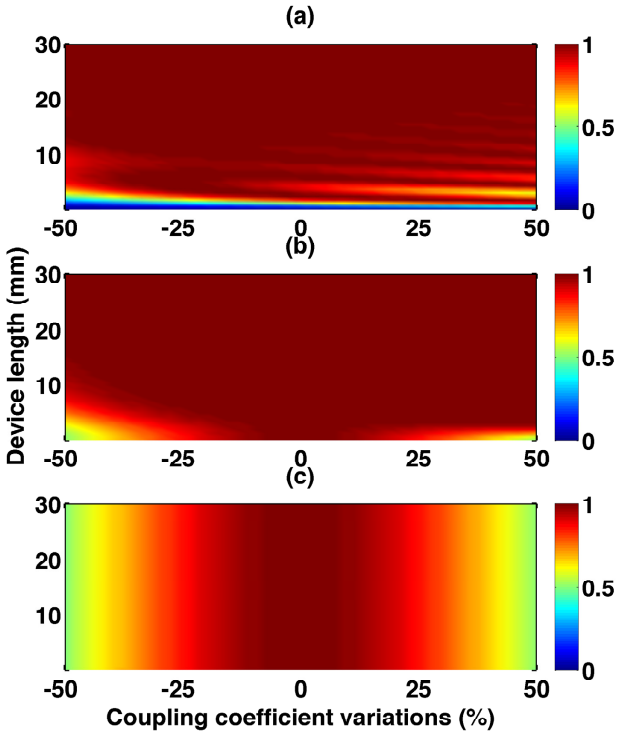

Fig. 5. Coupling efficiency against coupling coefficient variations for couplers designed using (a) adiabatic, (b) counterdiabatic, and (c) resonant coupling schemes.

#195633 - $15.00 USD Received 12 Aug 2013; accepted 19 Aug 2013; published 3 Sep 2013

4. Device design examples and beam propagation simulations

4.1. Simulation model

In the above analysis, we use numerical solutions of the coupled-mode equations to illustrate that one can start from an arbitrary adiabatic coupler design, applying the counterdiabatic formalism, and obtain the corresponding counterdiabatic coupler, which can be shortened beyond the adiabatic limit and ensures perfect fidelity. In this section, we illustrate the design of adiabatic waveguide couplers and their corresponding counterdiabatic couplers in a conventional planar integrated optics platform and perform beam propagation method (BPM) simulations to verify the designs. The scalar 2D BPM code used in the simulations solves the scalar and paraxial wave equation using the finite difference scheme with the transparent boundary condition [19]. We choose a polymer channel waveguide structure for beam propagation simulations. Similar structures have been experimentally demonstrated by photolithography and reactive-ion etching (RIE) [20]. The design parameters are chosen as follows: 3 μm thick SiO_2 (n =1.46) on a Si ($n = 3.48$) wafer is used for the bottom cladding layer, the core consists of a 2.4 μm layer of BCB ($n = 1.53$), and the upper cladding is epoxy ($n = 1.50$). The device is simulated at 1.55 μm input wavelength and the TE polarization. Subsequent waveguide design and BPM simulations are performed on the 2D structure obtained using the effective index method. For the chosen waveguide system, the relation between the mismatch Δ and width difference δW can be approximated by a linear relation [21], and the relation between the coupling coefficient κ and waveguide separation D in a symmetric coupler is well fitted by the exponential relation $\kappa = k_0 \exp[-\gamma(D - D_0)]$ [18]. We also assume that the exponential relation can be used to obtain an estimation of the coupling coefficient in the asymmetric coupler [21]. While a mode solver could be used to determine the coupling coefficient and mismatch precisely without the above approximations, we use these approximate forms in our device design for their convenience and to demonstrate that the proposed counterdiabatic formalism can be tolerant to possible waveguide parameter imperfections resulting from these approximations as discussed in section 3.3. The devices considered are weakly coupled, such that the system evolution can be described by the superposition of the unperturbed modes of the individual waveguides using the coupled-mode theory as in (1). So, the counterdiabatic protocol can be applied.

4.2. $L = 5$ mm devices

To verify the calculations in the previous section, we first design an adiabatic coupler using the parameters shown by the dash-dotted lines in Fig. 3(a). The design result is shown in Fig. 6(a). The geometry of the adiabatic mode-evolution coupler is determined by adjusting the relative separation between the waveguides and the waveguide widths to satisfy $\kappa = \kappa_0 \sin(\pi z/L)$ and $\Delta = \kappa_0 \cos(\pi z/L)$ with $\kappa_0 = 1$ mm^{-1} and $L = 1$ mm. As explained in section 3.1, this design, even though not being the best possible taper function, minimise the coupling between the eigenmodes because the separation of the eigenvalues is the maximum value allowed by the system throughout the evolution. We excite the lower waveguide by its unperturbed mode at $z = 0$, and the BPM result is shown in Fig. 6(a). The corresponding waveguide power evolution obtained by the overlap integral of the propagating field and the unperturbed waveguide modes is shown in Fig. 6(b). The result agrees very well with the coupled-mode equation solution shown by the dash-dotted lines in Fig. 2(a). Next, we design the corresponding counterdiabatic coupler using the parameters shown by the solid lines in Fig. 3(a). The design result is shown in Fig. 7(a). We note that, as illustrated in Fig. 3, the coupling coefficient and mismatch of the adiabatic coupler and the corresponding counterdiabatic coupler are different, thus their device geometries are different in Fig. 6 and Fig. 7. We again excite the lower waveguide by its unperturbed mode at $z = 0$, and the BPM result and the corresponding waveguide power evolution are

#195633 - $15.00 USD Received 12 Aug 2013; accepted 19 Aug 2013; published 3 Sep 2013

shown in Fig. 7. The power evolution in Fig. 7(b) again agrees very well with the coupled-mode equation solution shown by the solid lines in Fig. 2(a). The counterdiabatic coupler in Fig. 7 is the optimised design corresponding to the adiabatic coupler in Fig. 6, showing the properties of an ideal adiabatic coupler by following the theoretical eigenmode power evolution.

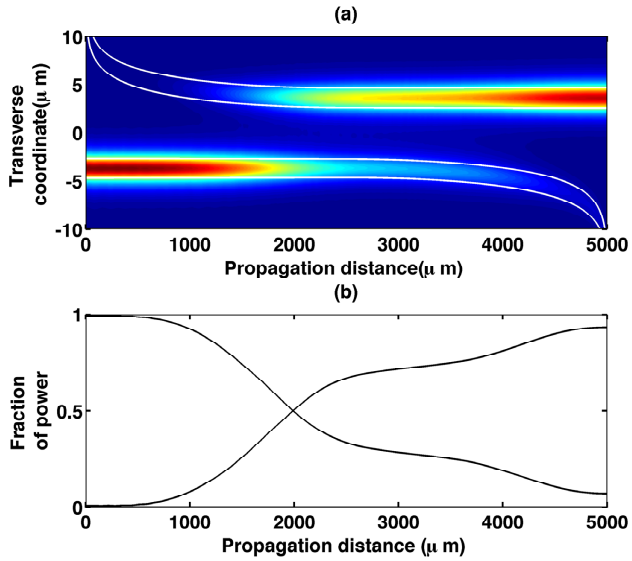

Fig. 6. (a) Waveguide geometry and BPM simulation of light propagation in a 5 mm adiabatic coupler. Solid white lines indicate the waveguide cores. (b) Fractional power evolution in the two waveguides.

4.3. $L = 500\mu m$ devices

Next, we consider an extreme case by reducing the device length by ten-folds to $L = 500\ \mu$m, and the coupling coefficient and mismatch of the adiabatic coupler still obey $\kappa = \kappa_0 \sin(\pi z/L)$ and $\Delta = \kappa_0 \cos(\pi z/L)$ with $\kappa_0 = 1\ \text{mm}^{-1}$. The resulting adiabatic coupler and the corresponding counterdiabatic coupler are shown in Fig. 8. We also show the BPM results in the couplers by exciting the lower waveguides by their unperturbed modes at $z = 0$. Clearly, this adiabatic coupler design in Fig. 8(a) is a bad one, and the coupling efficiency to the upper waveguide is low due to violation of the adiabatic condition $L \gg \frac{\pi}{2}$ mm. For the corresponding counterdiabatic coupler in Fig. 8(b), power is transferred to the upper waveguide according to the counterdiabatic formalism. This example clearly shows that the counterdiabatic formalism works by the additional coupling term $\mathbf{H}_{cd}$, with the additional coupling strength evident from the closer waveguide spacing in the counterdiabatic coupler in Fig. 8(b) as compared to the adiabatic coupler in Fig. 8(a). Started with a bad adiabatic design, the counterdiabatic formalism has successfully generated a short and high-fidelity counterdiabatic coupler.

We conclude this section by noting that the adiabatic coupler and its corresponding counterdiabatic coupler have different geometries because they have different coupling coefficients and mismatches. The counterdiabatic coupler can be regarded as an optimised design of the corresponding adiabatic coupler, possessing the properties of an ideal adiabatic coupler at short length and with high-fidelity.

#195633 - $15.00 USD Received 12 Aug 2013; accepted 19 Aug 2013; published 3 Sep 2013

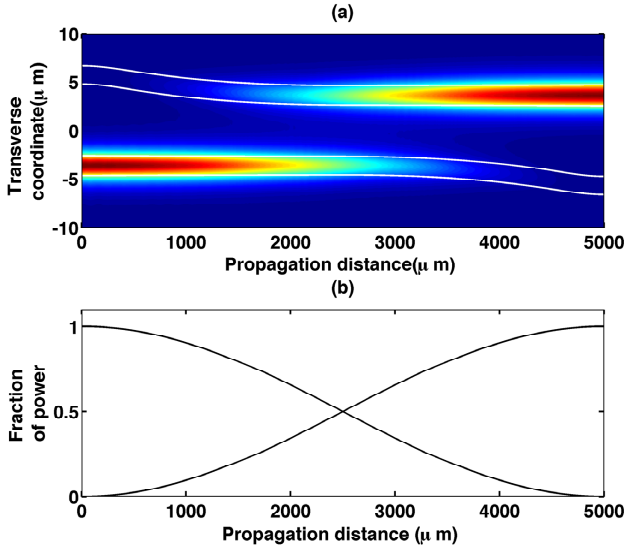

Fig. 7. (a) Waveguide geometry and BPM simulation of light propagation in a 5 mm counterdiabatic coupler designed by applying the counterdiabatic formalism to the adiabatic coupler in Fig. 6(a). Solid white lines indicate the waveguide cores. (b) Fractional power evolution in the two waveguides.

5. Discussion and conclusion

We used numerical solution of the coupled-mode equations and BPM simulations to show that the counterdiabtic formalism can be used to design short and high-fidelity waveguide couplers. Although only a particular taper design function for the adiabatic couplers is discussed in the examples, the focus is to illustrate theoretically and numerically the idea of the counterdiabatic formalism and its application to mode-evolution based coupled-wave devices, rather than the comparison of particular design approaches. Better taper functions can be found for the adiabatic devices [2, 21], however, the devices still work under the adiabatic approximation. On the other hand, the counterdiabatic formalism can be applied to any adiabatic design, and the resulting counterdiabatic device will follow exactly the adiabatic modes of the original design.

In the theoretical analysis, only two guided modes are considered. For a coupled-mode device with more than two guided modes, it is analogous to a multistate quantum system [22], and the counterdiabatic protocol can be directly implemented. For example, a shortcut to mode conversion in a multimode waveguide involving three guided modes has been demonstrated [13]. For planar coupled waveguide systems such as the one considered in Fig. 1, direct application of the counterdiabatic protocol results in coupling terms that are not physically realisable. In this paper, we demontrated that the imaginary coupling term can be eliminated by a proper unitary transformation for a two modes system, thereby rendering the design realisable with coupled waveguides. Whether a similar basis rotation exists for coupled waveguide system with more then two modes remains a subject of further research. The inclusion of other waveguide design considerations, such as the radiation mode and its analogy with a state that can decay, into the analysis and subsequent application of the fast and high-fidelity quantum driving protocols also requires further investigation.

In conclusion, we have derived a universal formalism for the design of short and high-fidelity mode-evolution based coupled-waveguide devices using the counterdiabatic protocol

#195633 - $15.00 USD Received 12 Aug 2013; accepted 19 Aug 2013; published 3 Sep 2013

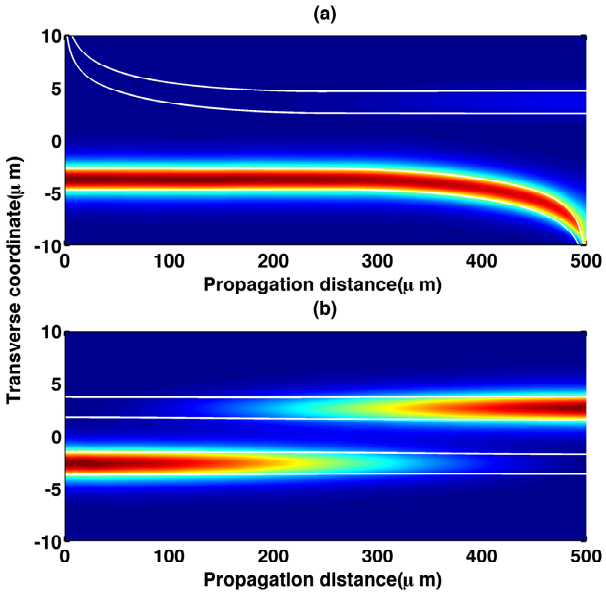

ti

Fig. 8. (a) Waveguide geometry and BPM simulation of light propagation in a 500 μm adiabatic coupler. Solid white lines indicate the waveguide cores. (b) Waveguide geometry and BPM simulation of light propagation in the corresponding 500 μm counterdiabatic coupler. Solid white lines indicate the waveguide cores.

and proper unitary transformation. A geometrical interpretation of the physical origin of the unitary transformation is given. Numerical calculations and BPM simulations agree with the theory. Tolerance analysis shows that the counterdiabatic devices combines the advantages of adiabatic and resonant devices. Counterdiabatic couplers are designed using the formalism. The result is applicable to any coupled-wave devices that can be described by the scalar and paraxial wave equation.

Acknowledgments

This work was supported in part by the National Science Council of Taiwan under contracts NSC 100-2221-E-006-176-MY3 and NSC 102-3113-P-110-004.

#195633 - $15.00 USD Received 12 Aug 2013; accepted 19 Aug 2013; published 3 Sep 2013